Chapter 5

Hollow-core high RI sensing optical fiber SPR sensor

In this chapter, A hollow-core D-shaped optical fiber-based surface plasmon resonance (SPR) sensor for low-loss and highly sensitive liquid analytes detection is theoretically investigated. The gold (Au) metal nanolayer is coated on the cladding etched D- shaped flat surface to develop the plasmonic effect. I have found good linear results ($R^2 > 0.99$) in analytes RIs versus resonance wavelength for gold layers thicknesses for the analytes RIs range of 1.45-1.52. This hollow core D-shaped optical fiber sensor achieves the maximum wavelength sensitivity of 23500 nm RIU^{-1} and a corresponding resolution of 4.26×10^{-6} RIU. I have obtained the maximum figure of merit (FOM) of 228 1/RIU. The proposed sensor may be highly active in detecting the biological and chemical liquid analytes.

5.1 Introduction

Nowadays surface plasmon resonance (SPR) technique is more attractive due to high sensitivity to the analytes refractive index (RI) with the contact of the metal layer. SPR shows more potential in chemical, biological, and physical sensing fields in surface-sensitive techniques due to real-time and level-free detection[183] [88] [155] Different types of SPR sensors are designed based on optical fiber, photonic crystal fiber (PCF) and Kretschmann-Reather prism, etc. The prism-based SPR sensors[184] can obtain good performance results but have many demerits, like being bulky, limited mechanical reliability, difficult for remote sensing, and expensive integration. Based on PCF and optical fiber SPR sensors have highly impactful due to electromagnetic immunity, network compatibility, and chemical inertness. In recent years, for different applications, various types of PCF and optical fiber sensors have been designed, such as D-shape fiber SPR sensors [185], hollow core fiber SPR sensors [185] [186] [187], long-period grating SPR sensors [188] tilted Bragg grating fiber SPR sensor [189] and Bragg grating fiber SPR sensor[190]. All sensors are very sensitive to the temperature, RI, and humidity change in the external area. The SPR condition occurs when the core-guided mode matches the surface plasmon polariton (SPP) mode, some core mode energy transfers to the SPP mode due to coupling, and a peak shows at core mode loss spectra at resonance wavelength[191]. All modes' propagation constant values are affected by changes in the analyte RIs, so this methodology[147] is very useful for sensing the analytes in chemical and biological areas. Some optical fiber and PCF SPR sensors are designed theoretically and experimentally in this type that sensing liquid can hold inside the hole of the PCF or inside the hollow core of fiber which is coated by plasmonic metals. R. Nasirifar et al. proposed the temperature detection hollow-core optical fiber sensor in which optical fiber hollow-core walls had coated with silver (Ag) metal. A. Hassani et al.[191] investigated the SPR-based

microstructured RI detection optical fiber sensor in which the core of the optical fiber was coated with gold (Au) metal. X. Yang et al.[186] reported the sensor with graphene and Ag bilayer coated inside surfaces the core of the PCF. Liu et al.[191] reported a hollow-core Au-coated high RI detection optical fiber sensor. G. Luo et al.[192] proposed the Cu-coated hollow-core optical fiber sensor. The coating process of the metal film techniques is very complex and difficult to coat the inner walls of the hollow-core and holes surfaces of the optical fiber because the size of the hollow-core or holes of the optical fiber is microns range [186 191 192]. These SPR sensors also have challenges, such as detecting high RI liquid analytes and highly reactive liquid analytes. The analytes' RI detection limit of almost all silica-made SPR sensors is typically lower than 1.42 because analytes are filled in cladding holes of PCF-SPR sensors or filled in the out-of-cladding side region of optical fiber sensors. The RI of fiber must be higher than the RIs of analytes to sustain the fiber's total internal reflection (TIR) condition. The hollow-core optical fiber and hollow-core PCFs-based SPR sensors can solve the problem of high RIs analytes detection because liquid analytes fill the hollow-core of fiber in these types of sensors[192 122].

From the above discussion, it is clear that the solid-core optical fiber sensors[193] have a couple of inherent limitations. Firstly, they lack a built-in cavity for measuring the analyte, necessitating an external analyte cell or chamber. They have added complexity to the experimental setup and increased the risk of contamination or leakage. Secondly, solid-core optical fiber sensors are limited in detecting analytes with a refractive index higher than the fiber core due to the principle of total internal reflection. This restriction can limit the sensor's effectiveness in measuring analytes, as it restricts the range of analytes that can be effectively measured.

The fiber-based SPR sensors using PCF[122] or micro-structured optical fiber[192] (MOF) have recently garnered valuable attention. These types of SPR sensors offer exclusive

features and have the possibility to overcome some limitations of solid-core fiber sensors. PCF and MOF structures recognize greater flexibility in sensor design, such as introducing additional functional elements or creating specific hole patterns, which can enhance sensor performance. However, the complicated structures of PCF and MOF are challenging in SPR sensor fabrication. The precise control and intricate designs of the fiber structures require advanced fabrication methods.

Hollow-core fiber-based SPR sensors have emerged as a hopeful solution to overcome the shortcomings of solid-core fiber-based SPR sensors. The hollow core of these fibers can serve as an analyte chamber, allowing for direct placement of the analyte to be detected. These eliminate the need for external analyte cells and simplify the sensor setup. It can also measure higher RIs than the supporting cladding material. In addition to these advantages, hollow-core fiber SPR sensors typically have a more straightforward structure than PCF- or MOF-based SPR sensors, making them relatively easier to fabricate. Various configurations and designs of hollow fiber SPR sensors[193] [193] have been reported in the literature, versatility, and offering flexibility for various sensing applications. Overall, the use of hollow fiber SPR sensors represents a promising approach to addressing the shortcomings of solid core fiber sensors, offering improved analyte containment, expanded detection capabilities, and simplified fabrication processes.

I designed a very simple D-shaped structure SPR technique-based hollow-core optical fiber sensor to solve the above problem. The Au nanofilm is coated on the flat surface side-polished optical fiber. This sensor easily detects high refractive index analytes filled into the hollow core. Using the FEM technique, the sensor modeling, electric field distribution in different modes, and SPP and core mode matching are analyzed by COMSOL Multiphysics software. The light is guided in the analyte-filled hollow core,

and SPP mode is generated on the gold-coated D-shaped flat surface. The hollow-core SPR sensor achieves the maximum FOM 228 1/RIU, maximum sensitivity 23500 nmRIU^{-1}, and corresponding resolution 4.26 × 10^{-6} RIU for a 30 nm thick Au layer.

5.2 Design and sensing analysis

The schematic view of the cross-section image of a gold (Au) coated D-shaped hollow-core SPR sensor is demonstrated in Fig. (5.1). The hollow-core filled by analyte, fiber cladding fused silica, and coated Au layer are indicated by sky blue, orange, and yellow color, respectively. 50/125µm (hollow core/ outer cladding) diameter hollow-core optical fiber used in this sensor design. The side-polishing technique can be used to manufacture the D-shaped fiber. I have analyzed sensing for various thicknesses layers of gold-coated on a flat D-shaped surface of side-polished optical fiber. Separation (s = 0.1µm) is optimized between the Au layer surface and the hollow-core curve surface for no direct contact between the metal and analytes and strong coupling. The liquid analyte is filled in the hollow-core region at sensor operating time.

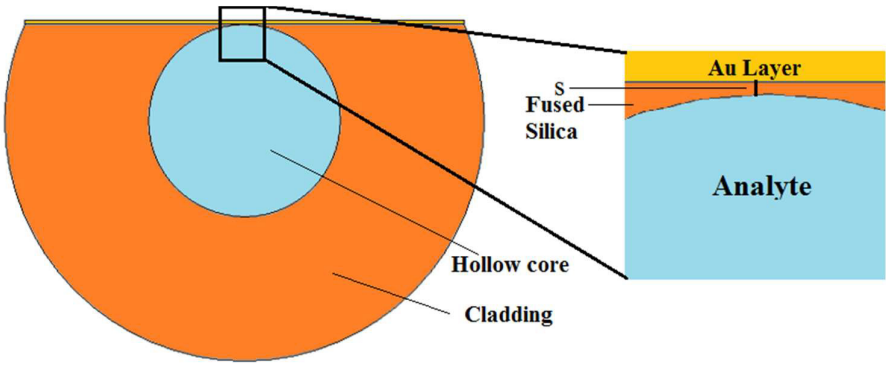

Fig. 5.1 Hollow core fiber SPR sensor cross-section view.

The wavelength-dependent RI of used fiber cladding fused silica is calculated using the dispersion relation of Sellmier's, [124]

$$n(\lambda) = \sqrt{1 + \frac{C_1\lambda^2}{\lambda^2 - D_1^2} + \frac{C_2\lambda^2}{\lambda^2 - D_2^2} + \frac{C_3\lambda^2}{\lambda^2 - D_3^2}} \tag{5.1}$$

Where λ (in μm) represents the wavelength, whereas C_1, C_2, C_3, D_1, D_2 and D_3 show the Sellmeir coefficients which are given in table 5.1.

Table 5.1 Sellmeir's coefficient values.

C_1	C_2	C_3	D_1(μm)	D_2(μm)	D_3(μm)
0.6961663	0.4079426	0.8974794	0.0684043	0.1162414	9.896161

The wavelength-dependent dielectric constant of used plasmonic metals is calculated by Eq. (5.2) using the Drude model[194]

$$\varepsilon_g(\lambda) = \varepsilon_{gr} + i\varepsilon_{gi} = \frac{\lambda^2\lambda_c}{\lambda_p^2(\lambda_c + i\lambda_p)} \quad (2)$$

Where, $\lambda_p(= 0.16826\ \mu m)$ and $\lambda_c(= 8.9342\ \mu m)$ represent plasma and collision wavelength, respectively for the gold metal. All used structural parameters of the proposed sensor are shown in table 5.2.

Table 5.2 Optimized parameters of designed sensor structure.

Parameter	**Size**
Fiber hollow-core diameter	50 μm
Fiber cladding diameter	125 μm
Separation between Au layer and hollow-core curve boundary (S)	0.1 μm
Optimized Au layer thickness (t)	30 nm

I have proposed a simple hollow-core D-shaped optical fiber structure, which can be easily fabricated using the most suitable techniques like stack and draw method[195], side polishing and laser micro-machine technique[124], micro-drilling technology[196] and high power fiber laser[197]. Additionally, the optical fiber D-flat surface can also be easily coated using the many authentic techniques like as chemical vapor deposition (CVD), high-

pressure micro-fluidic chemical deposition, atomic layer deposition (ALD)[103], magnetron sputtering deposition[196] and pulse laser deposition (PLD)[185]. Plasmonic material deposition on the D-flat surface is easier compared to the inside deposition of the hollow core due to the hollow-core size in the micron range.

5.3 Result and discussions

The proposed hollow-core sensor is based on a very sensitive technique SPR between mode and SPP mode. The designed hollow-core sensor loss is obtained from the effective index imaginary part value and defined as[101]

$$\alpha = 8.686 \times 10^4 . K_0 . Im(n_{eff}) \quad [dB/cm] \tag{5.3}$$

Where $K_0 (= 2\pi/\lambda)$, λ, and $Im(n_{eff})$ represent the wave number, working wavelength and coupling mode effective index imaginary part value[134], respectively.

The electric field distribution of the core, SPP, and coupling mode for the 30 nm Au layer at analyte RI of 1.45 and loss spectra for all layers of Au are shown in Fig.5.2. In this figure, the "core mode" represents the amount of energy that is guided within the core of the fiber. The "SPP mode" represents the energy associated with the surface plasmon wave at the metal-dielectric interface. The "coupling mode" represents the amount of energy that is transferred from the core mode to the SPP mode. I can see from Fig. 5.2 that loss values initially increase with wavelength; after a peak value, it does continue to decrease. I have observed that this peak value occurs at a specific wavelength where the core mode and SPP mode are perfectly matched, resulting in the maximum transfer of energy from the core mode to the SPP mode.

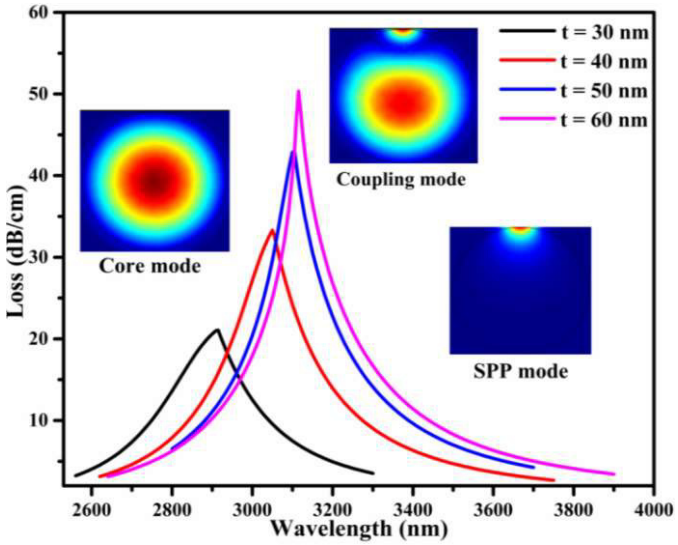

Fig. 5.2 The Electric field distribution inset of the core, SPP and coupling mode at an analyte RI n_a = 1.45 for a 30 nm Au layer. The loss spectra for all thicknesses (30 nm, 40 nm, 50 nm and 60 nm) layers of Au at $\boldsymbol{n_a = 1.45}$.

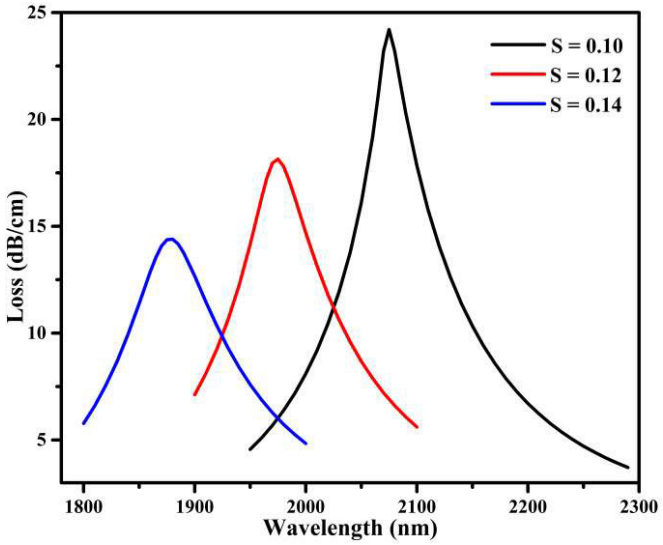

Fig. 5.3 The loss spectra at different separation between Au layer and hollow-core curve boundary (S) for 30 nm thick Au layer.

Fig. 5.3 represents the loss spectra with the wavelengths at different separation between Au layer and hollow-core curve boundary (S) at an analyte RI = 1.49. For lower boundary separation, I have found the maximum loss peak because at lower separation, evanescent wave is easily to penetrate and excite the gold nano layer electrons. So, I have chosen lower boundary separation optimized parameter S = 0.10 for strong coupling.

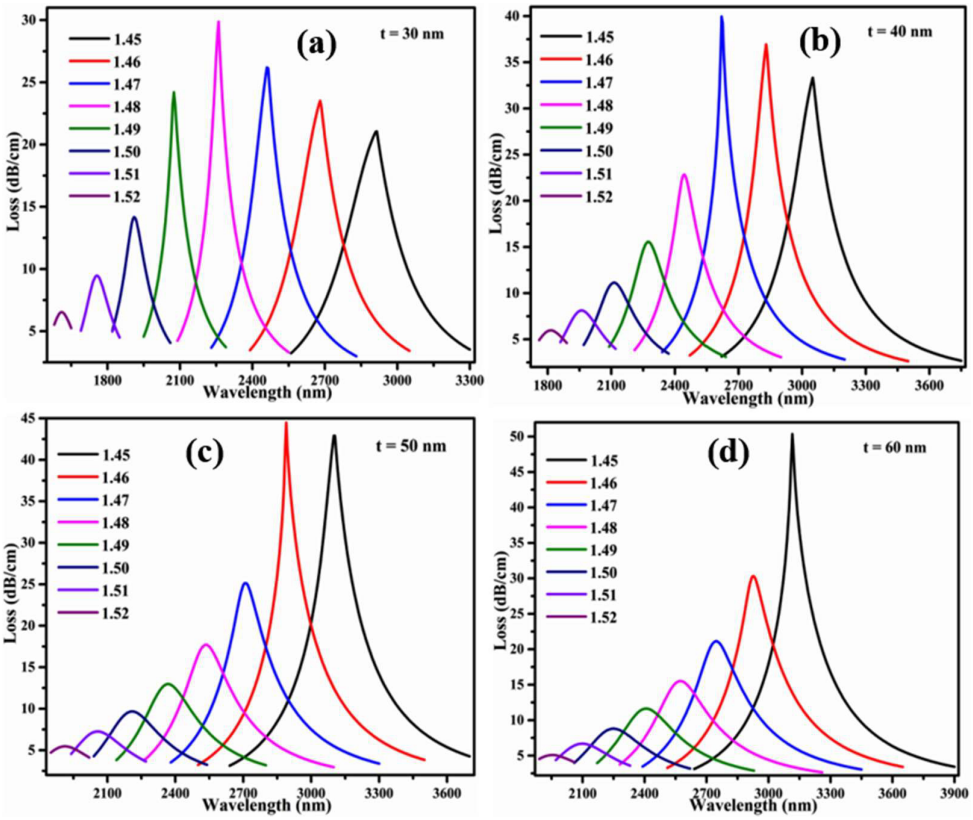

Fig. 5.4 (a-d) the loss spectra at t = 30 nm, t = 40 nm, t = 50 nm and t = 60 nm for analytes range $\boldsymbol{n_a}$ = 1.45-1.52.

Figs. 5.4(a)-(d) illustrate the variation of core loss spectra for all thick gold layers in the liquid analytes RI range of 1.45-1.52. From Figs.5.4 (a)-(d), i can see that the loss spectra's behavior change with the Au layer thickness (t). The loss peak values for the 30 nm thick Au layer initially increase with analytes RIs (n_a = 1.45-1.48); after, it continues to decrease till RI n_a = 1.52. The loss peak values for the 40 nm thick Au layer initially increase with analytes RIs (n_a = 1.45-1.47 and then continue to decrease till RI n_a = 1.52. For the 50 nm thick Au layer, the loss peaks increase with RIs (n_a = 1.45-1.46); for RIs ranges (n_a= 1.46 -1.52), the peaks values decrease continuously. For the 60 nm thick Au layer, the loss peak values decrease continuously with analyte RIs range n_a = 1.45-1.52. The proposed SPR sensors are very sensitive to the analyte RI. For a fixed analyte RI, the loss values initially increase with the wavelengths, and after a resonance peak value, it

sharply decreases. I have taken the simulation results from data values for minimum separation steps of wavelengths. So, i have found the sharpness in the plots for every analyte RIs, as shown in Fig 5.4.

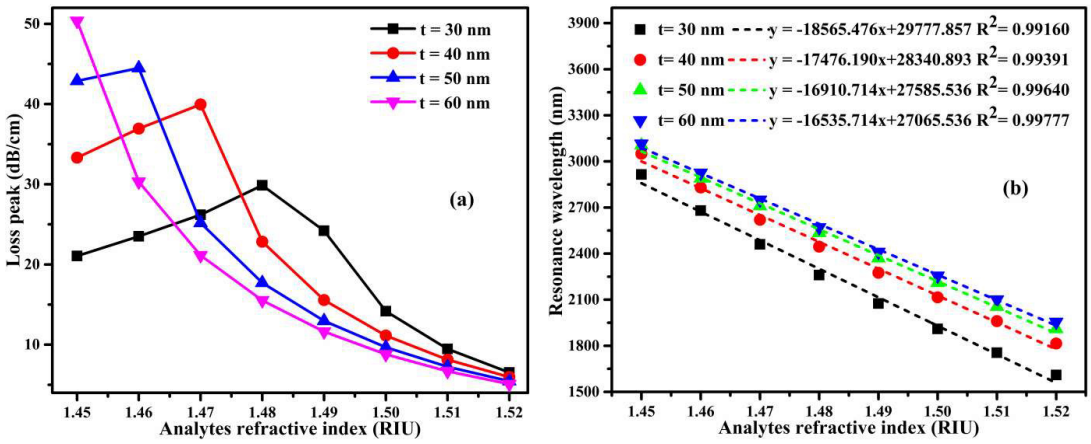

Fig. 5.5 (a) The loss peak value spectra **(b)** The resonance wavelength versus analytes RIs (n_a=1.45-1.52) for different thick (t) Au layers.

Fig. 5.5 (a) shows the effect in peak values by analytes RIs for different thick Au layers. Fig. 5.5 (b) reveals the variation in peak value resonance wavelength with liquid analytes RIs for all gold layers thicknesses. It is clear from Fig. 5.5(b) that if I increase liquid analytes RIs, the resonance wavelength values shift to a blue wavelength side for all gold layers. The resonance wavelength values shift to a higher wavelength side with the Au layers thicknesses (t) at a fixed analyte refractive index. I have found good linear (R^2>0.99) plots of resonance wavelengths with analytes RIs for all gold layers thicknesses.

The change in liquid analytes RIs (Δn_a) is obtained by calculating the shifting values ($\Delta\lambda_{peak}$) of the resonance wavelength peak in the core mode loss spectra. The sensor performance parameter wavelength sensitivity is obtained by using the WIM method[198]. It is defined as given below.

$$S_\lambda = \Delta\lambda_{peak}/\Delta n_a \; [nm/RIU] \tag{5.4}$$

Another important hollow-core sensor parameter is the full width at half maxima resonance bandwidth. This parameter represents the pulse of the SPR. The maximum sensitivity and smaller bandwidth translate into the best accuracy of the proposed sensor. The figure of merit (FOM) performance parameter of the hollow-core sensor is obtained by the sensitivity and FWHM resonance bandwidth ratio. It is defined as

$$FOM \; = S_\lambda/FWHM \; [1/RIU] \tag{5.5}$$

Figs. 5.6(a) and (b) show the wavelength sensitivity and FOMs of the designed hollow-core sensor with analytes RIs changing from 1.45 to 1.52 for all gold layers, respectively. I can see from Fig. 5.6(a) that the wavelength sensitivity decreases with the analyte RIs for all Au layer thicknesses. Fig. 5.7 depicts the maximum sensitivity and FOM variations with gold layer thicknesses. The maximum sensitivities of the designed hollow-core sensor are 23500 $nmRIU^{-1}$, 22000 $nmRIU^{-1}$, 21500 $nmRIU^{-1}$, and 19000 $nmRIU^{-1}$, respectively, for 30 nm to 60 nm Au layers thicknesses (t) at the analyte RI (n_a) 1.45. Maximum FOMs are 228.00 1/RIU, 178.12 1/RIU, 142.74 1/RIU, and 139.92 1/RIU, respectively, at analytes RIs n_a 1.48, 1.47, 1.46, and 1.45 for 30 nm to 60 nm gold layers thicknesses (t). The sensitivity of the sensor is represented by the ratio of the resonance wavelength shifting and analyte refractive index changes. The resonance wavelength shifting values decrease with increasing analyte refractive indices. The variations in resonance wavelength and figure of merit also change due to changes in the coupling effect with the Au layer thicknesses. The ratio of the sensitivity and FWHM reveals the figure of merit of the sensor. Hence, I obtain a slightly random trend in the variations of the figure of merit due to changes in the sensitivity and FWHM.

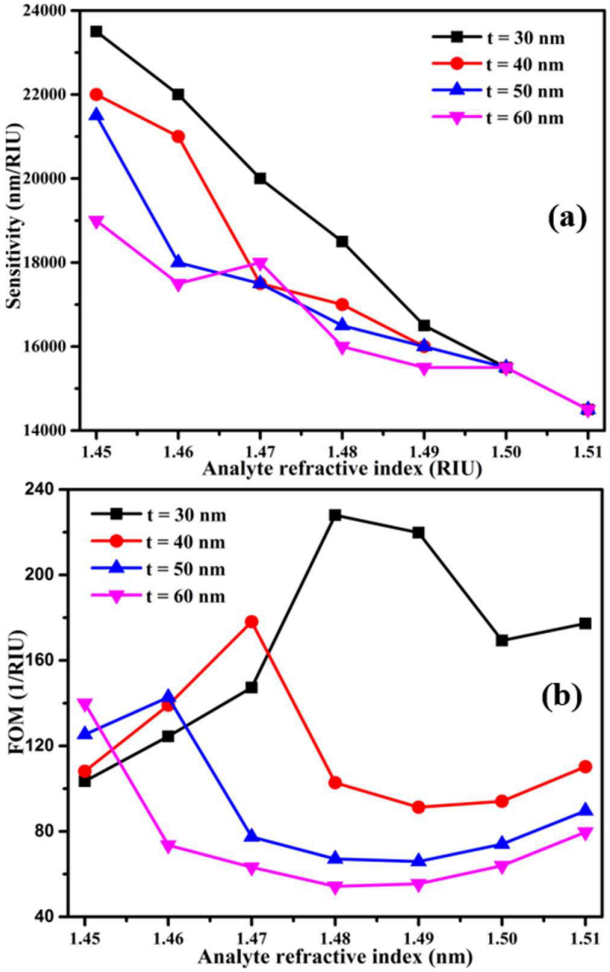

Fig. 5.6 (a) The sensitivity's **(b)** FOMs of the investigated hollow-core sensor for analytes RIs change from 1.45 to 1.52 for all Au layers (t).

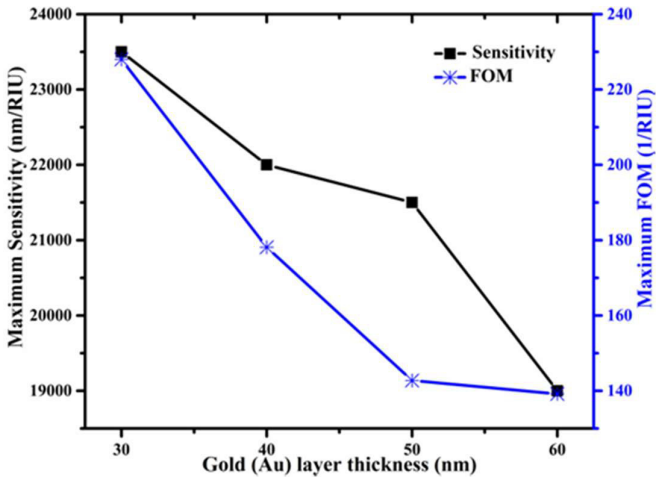

Fig. 5.7 The maximum sensitivities and FOMs variation with the Au layers thickness.

One another important performance parameter is the "resolution" of the designed hollow-core sensor that represents the minimum variation sensing in analyte RI in real-time. The resolution of investigated hollow core sensor can be computed using equation (5.6)[199]

$$R = \frac{\Delta\lambda_{min}}{\Delta\lambda_{peak}} \times \Delta n_a[RIU] \quad (5.6)$$

If considered 0.1 nm minimum spectral resolution ($\Delta\lambda_{min}$), then I found the resolution in the 10^{-6} order, which means my hollow-core designed sensor can detect the 10^{-6} order analyte RIs variations.

Table 5.3 Performance parameters results of the designed hollow-core sensor for a 30 nm thick Au layer.

Analyte (RIU)	Loss Peak (dB/cm)	Resonance Wavelength (nm)	Wavelength Shift (nm)	Sensitivity (nmRIU^{-1})	FWHM (nm)	FOM (1/RIU)
1.45	21.051	2915	235	23500	227.15	103.46
1.46	23.512	2680	220	22000	176.76	124.46
1.47	26.199	2460	200	20000	135.80	147.28
1.48	29.871	2260	185	18500	81.14	228.00
1.49	24.206	2075	165	16500	75.07	219.79
1.50	14.170	1910	155	15500	91.55	169.30
1.51	9.470	1755	145	14500	81.80	177.26
1.52	6.536	1610	-	-	42.25	-

Table 5.4 Comparison of my designed hollow-core sensor with other hollow-core optical fiber-based RI sensors.

Reference	Maximum Sensitivity ($nmRIU^{-1}$)	Resolution (RIU)	FOM (1/RIU)	RI range
200	4350	-	149	138-1.49
199	12400	1.61×10^{-6}	-	1.46-1.48
181	6974	-	-	1.30-1.35
192	7111	- -	-	1.5094-1.5801
201	10570		97.88	1.30-1.41
199	14996.81	-	139.78	1.28-1.44
This work	23500	4.26×10^{-6}	228	1.45-1.52

The loss peak, resonance wavelength, wavelength shift, sensitivity, FWHM, and FOM parameters resulting from my hollow-core designed sensor for a 30 nm thick Au-coated layer are shown in Table 3. The maximum sensitivity, resolution, FOM, and RI-range performance parameters comparison between the proposed hollow-core RI sensor and other last year's published articles are shown in Table 5.4.

5.4 Conclusion

In conclusion, I have proposed and investigated a very simple D-shaped structure SPR high RI sensor based on hollow-core optical fiber. The gold (Au) metal is deposited on the flat D-shaped fiber surface. The FEM technique is used for all fiber modes calculating and analyzing. My hollow-core sensor model design can offer more benefits than previously reported optical fiber sensors, such as a simple and cheaply made metal coating facility, high RI analytes detecting, and sensing execution in real time. I have evaluated sensor performance in the analytes RIs range 1.45-1.52 by analyzing the loss peak position sifting. At the optimized 30 nm thick Au layer, I have found maximum

sensitivity of 23500 $nmRIU^{-1}$ and a corresponding resolution of 4.26×10^{-6} RIU. My hollow-core sensor is designed in this type with no direct contact between metal and analyte, so some highly active biological and chemical liquid analytes can also be detected by using it.